Channel and wedge plasmon modes of metallic V-grooves with finite metal thickness

José Dintinger and Olivier J.F. Martin
Nanophotonics and Metrology Laboratory Swiss Federal Institute of Technology Lausanne (EPFL)
EPFL-STI-NAM, ELG Station 11 CH-1015 Lausanne, Switzerland
www.nanophotonics.ch
**Corresponding author: jose.dintinger@epfl.ch*

Abstract: We investigate numerically the effect of a finite metal film thickness on the propagation characteristics of the channel plasmon polariton (CPP) and wedge plasmon polariton (WPP) modes, both in a symmetric and asymmetric environment. We observe that decreasing the metal thickness results in an improvement of the field localization near the groove tip and an increase of the losses for both types of mode. This behavior stems from the typical symmetric charge distribution of both modes across the metal film. When considering an asymmetric dielectric environment, the CPP mode is found to evolve into short range plasmon modes propagating along the groove walls, in contrast to the WPP mode which remains essentially confined at the tip apex. These results can be useful to tailor the properties of such plasmon modes, using the metal thickness as the variable parameter.

OCIS codes: (240.6680) Surface plasmons; (240.0310) Thin films ; (230.7380) Waveguides, channeled.

References and links

1. A. Fulbert and T. Pearsall, "A European roadmap for photonics and nanotechnology," MONA, Merging Optics & Nanotechnologies (2008).
2. E. Ozbay, "Plasmonics: Merging photonics and electronics at nanoscale dimensions," Science **311**, 189-193 (2006).
3. W. L. Barnes, A. Dereux, and T. W. Ebbesen, "Surface plasmon subwavelength optics," Nature **424**, 824-830 (2003).
4. J. T. Kim, J. J. Ju, S. Park, M.-s. Kim, S. K. Park, and M.-H. Lee, "Chip-to-chip optical interconnect using gold long-range surface plasmon polariton waveguides," Opt. Express **16**, 13133-13138 (2008).
5. S. Sidorenko, and O. J. F. Martin, "Resonant tunneling of surface plasmon-polaritons," Opt. Express **15**, 6380-6388 (2007).
6. H. Raether, "Surface-Plasmons on Smooth and Rough Surfaces and on Gratings," Springer Tracts Mod. Phys. **111**, 1-133 (1988).
7. T. W. Ebbesen, C. Genet, and S. I. Bozhevolnyi, "Surface-plasmon circuitry," Phys. Today **61**, 44-50 (2008).
8. A. Boltasseva, V. S. Volkov, R. B. Nielsen, E. Moreno, S. G. Rodrigo, and S. I. Bozhevolnyi, "Triangular metal wedges for subwavelength plasmon-polariton guiding at telecom wavelengths," Opt. Express **16**, 5252-5260 (2008).
9. S. I. Bozhevolnyi, V. S. Volkov, E. Devaux, and T. W. Ebbesen, "Channel plasmon-polariton guiding by subwavelength metal grooves," Phys. Rev. Lett. **95**, 046802 (2005).
10. S. I. Bozhevolnyi, V. S. Volkov, E. Devaux, J. Y. Laluet, and T. W. Ebbesen, "Channel plasmon subwavelength waveguide components including interferometers and ring resonators," Nature **440**, 508-511 (2006).
11. D. K. Gramotnev and D. F. P. Pile, "Single-mode subwavelength waveguide with channel plasmon-polaritons in triangular grooves on a metal surface," Applied Physics Letters **85**, 6323-6325 (2004).
12. D. K. Gramotnev and K. C. Vernon, "Adiabatic nano-focusing of plasmons by sharp metallic wedges," Applied Physics B-Lasers and Optics **86**, 7-17 (2007).
13. E. Moreno, F. J. Garcia-Vidal, S. G. Rodrigo, L. Martin-Moreno, and S. I. Bozhevolnyi, "Channel plasmon-polaritons: modal shape, dispersion, and losses," Opt. Lett. **31**, 3447-3449 (2006).

#105456 - $15.00 USD Received 17 Dec 2008; revised 30 Jan 2009; accepted 30 Jan 2009; published 5 Feb 2009

14. E. Moreno, S. G. Rodrigo, S. I. Bozhevolnyi, L. Martin-Moreno, and F. J. Garcia-Vidal, "Guiding and focusing of electromagnetic fields with wedge plasmon polaritons," Phys. Rev. Lett. **100**, 023901 (2008).
15. I. V. Novikov and A. A. Maradudin, "Channel polaritons," Phys. Rev. B **66**, 035403 (2002).
16. S. I. Bozhevolnyi, "Effective-index modeling of channel plasmon polaritons," Opt. Express **14**, 9467-9476 (2006).
17. E. D. Palik, *Handbook of Optical Constants of Solids* (Academic, New York 1985).
18. D. K. Gramotnev, "Adiabatic nanofocusing of plasmons by sharp metallic grooves: Geometrical optics approach," J. Appl. Phy. **98** (2005).
19. COMSOL Multiphysics version 3.4.
20. M. Yan and M. Qiu, "Guided plasmon polariton at 2D metal corners," J. Opt. Soc. Am. B-Opt. Phys. **24**, 2333-2342 (2007).
21. J. Chen, G. A. Smolyakov, S. R. J. Brueck, and K. J. Malloy, "Surface plasmon modes of finite, planar, metal-insulator-metal plasmonic waveguides," Opt. Express, 14902-14909 (2008).
22. E. N. Economou, "Surface Plasmons in Thin Films," Phys. Rev. **182**, 539-554 (1969).
23. J. J. Burke, G. I. Stegeman, and T. Tamir, "Surface-polariton-like waves guided by thin, lossy metal films," Phys. Rev. B **33**, 5186 (1986).
24. J. Van Bladel, *Singular electromagnetic fields and sources* (Oxford Univ. Press, Oxford 1995).
25. L. D. Landau and E. M. Lifshitz, *Electrodynamics of continuous media* (Pergamon Press, Oxford 1984).
26. R. Zia, M. D. Selker, and M. L. Brongersma, "Leaky and bound modes of surface plasmon waveguides," Phys. Rev. B **71**, 165431 (2005).

1. Introduction

The constant need for faster signal processing systems has recently driven the information technology industry to consider the possibility of implementing optical interconnects in electronic circuits to achieve faster clock distribution and interdevice communication [1]. This approach has however been hampered by the size mismatch between electronic and photonic components. The size of the latter is indeed restricted by the so-called diffraction limit which imposes dimensions in the order of the light wavelength, i.e. typically a hundred times larger than those of electronic components. Surface plasmon-based photonics, i.e. plasmonics, has recently appeared as one of the most promising technological solutions to these stringent requirements by offering the possibility to guide light in the form of surface plasmon (SP) waves on metallic structures [2-5]. Indeed, SPs, which are surface waves propagating at the boundary between a dielectric and a metal, make possible the confinement of light to subwavelength volumes as a result of its interaction with the free electrons of the metal (the SP fields decaying exponentially away from the interface in both media) [6].

Over the past years, much effort has been devoted to the development of a robust plasmonic circuitry for routing and processing SP signals [2, 7]. One of the main challenges addressed is the realization of low-loss guiding structures capable of confining the SP waves laterally to make them compatible with high integration configurations. Among the broad variety of plasmonic waveguides that have been proposed so far, metallic V-shaped grooves and wedges have recently attracted much attention [8-15]. Both theoretical [11-14, 16] and experimental studies [8, 9] have shown that the bound modes supported by such structures, i.e the channel plasmon-polariton mode (CPP) and wedge plasmon-polariton mode (WPP), can provide relatively long propagation lengths combined with a strong mode confinement. Several waveguide components based on these geometries have already been demonstrated: Mach-Zender interferometers or ring resonators [10]. While the influence of various geometric parameters (groove and wedge angle, depth, curvature angle) has been studied in detail, none of the work done so far has considered the role of the metal thickness. We can, however, expect that this parameter will considerably affect the propagation and mode confinement of both CPP and WPP modes. It should therefore provide an additional degree of freedom which can be easily controlled by the fabrication process. This can be particularly interesting for the nanoimprint lithography technique, recently introduced for the fabrication of such structures [8], where metallic films are deposited in preformed grooves (in contrast to focused ion beam milled structures where the grooves were etched in bulk metal [9]).

In this paper, we investigate in detail the effect of the metal film thickness on the propagation characteristics of CPP and WPP modes by considering a V-shaped gold film with

#105456 - $15.00 USD Received 17 Dec 2008; revised 30 Jan 2009; accepted 30 Jan 2009; published 5 Feb 2009

finite thickness as the guiding structure. The complex propagation constants and mode profiles are obtained for different thicknesses and wavelengths using the finite-element method. We first consider a symmetric environment for which the metallic film is embedded in air, and then study the effect of the dielectric contrast between the substrate and the superstrate media.

2. Geometry and modal analysis

The geometry, shown in Fig. 1(a), is a gold film of thickness *t* shaped into a V-groove, infinitely long in the z-direction and surrounded by dielectric media characterized by their permittivity ε_1 and ε_2, or refractive indices n_1 and n_2. The complex permittivity ε_{Au} of the metal is obtained by fitting the experimental values from [17] with a polynomial curve. In the following, medium 1 will be referred as the core medium and medium 2 as the cladding medium when discussing the CPP mode, and vice versa when discussing the WPP mode. All the corners in the structure are rounded to avoid field singularities using a fixed 10 nm curvature radius for the inner corners while the curvature radius of the outer corners is adjusted to (10+*t*) nm to keep the metal thickness constant at the corners, Fig. 1(a). The depth of the groove is chosen to be 5 microns and the groove angle 25°; these values are chosen according to previous studies in order to avoid any cut-off related to these geometric parameters in the considered wavelength range (0.7-1.6 μm) [12-14, 18]. The modal analysis is carried out with the finite-element method using the commercial software Comsol [19]. In order to reduce the computation effort, we take advantage of the known symmetry of the CPP and WPP modes by setting an electric wall (Ey=0) and a magnetic wall (Hy=0) respectively, along the y-axis at the center of the structure. The size of the computation domain is then 10x5 μm^2 and the number of unknowns is on the order of $5x10^5$ with a mesh size of 2 nm close to the tip. Perfectly matched layers (PML) were added at the boundaries of the computation domain to simulate an open space and eliminate reflections at the boundaries of the computation domain.

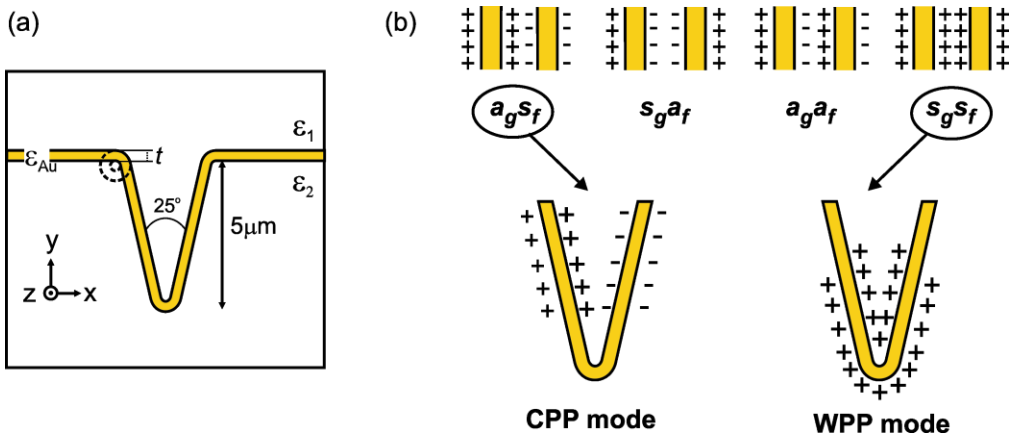

Fig. 1. (a) Sketch of the simulated structure. (b) Symmetries of the charge distribution associated with the different SP coupled modes for two thin films and the corresponding CPP and WPP modes. The symmetry of a mode is described with a symbol α_β with α=*s*, respectively *a*, for symmetric, respectively antisymmetric charge distributions across the gap (β=*g*) or the film (β=*f*).

An obvious consequence of considering a finite metal thickness is that our structure supports both CPP and WPP modes at the groove apex. High-order CPP modes extending on the groove sides can also exist as a consequence of the large groove depth, but in the following we will only focus on the fundamental CPP mode and on the single WPP mode supported by the structure [20]. Besides these modes confined at the apex, the top corners may

#105456 - $15.00 USD Received 17 Dec 2008; revised 30 Jan 2009; accepted 30 Jan 2009; published 5 Feb 2009

also support additional WPP modes (but not CPP modes which are not allowed due to the wide angle of 102.5 ° formed by the top corners). Finally, the groove walls can act as strip waveguides supporting SP modes confined laterally by the top and bottom corners [8] while the horizontal metal film can support SP modes extending infinitely in the x-direction.

In order to gain a better understanding of the origin and field distribution of the CPP and WPP modes in our structure, it can be useful to first consider the SP modes supported by a simpler structure consisting of two infinite parallel thin metal films embedded in a dielectric medium, Fig. 1(b). CPP and WPP modes can indeed be analyzed on the basis of the coupled modes formed by two SP modes propagating toward the tip on the opposite faces of the groove or wedge [12, 18]. By considering the two conceivable SP coupling symmetries for a bulk groove (wedge), it can be shown that only the mode with an antisymmetric (symmetric) charge distribution across the groove (wedge) can produce the CPP (WPP) mode. The reason for this is that the other coupling symmetry leads to a mode which effective index decreases when the distance between the two opposite surfaces is reduced, i.e when the two SP waves approach the tip of the structure. By extending this analysis to our thin film geometry, we must consider the four SP modes sketched in Fig. 1(b) which correspond to the different coupling symmetries possible across the dielectric gap and across the metallic films [21, 22]. These modes are characterized by distinct symmetries of their field and charge distributions across the film *and* across the gap, and can be denoted accordingly [see Fig. 1(b)]. The modes $a_g s_f$ and $s_g a_f$ correspond to gap SP modes with their field concentrated in the gap [21] and are likely to form CPP modes. However, for the same reasons mentioned above, only the mode showing an antisymmetric charge distribution across the gap ($a_g s_f$) is expected to give rise to the CPP mode. The two other coupled modes $a_g a_f$ and $s_g s_f$ have their field mainly located in the cladding (outside the gap) [21] but only the one showing a symmetric charge distribution with respect to the groove axis ($s_g s_f$) gives rise to the WPP mode [Fig.1(b)]. A common feature of the CPP and WPP mode is therefore the symmetric charge distribution across each individual metallic layer: they can be described as the symmetric and antisymmetric combination of symmetric (or short range, SRP) surface plasmon modes propagating on each sidewall. We will see in the following that their modal behavior with respect to the metal thickness is indeed reminiscent of that of the SRP mode of extended thin films [23].

These considerations on the charge distribution are confirmed by the electric field distribution of the modes found in our simulations which are presented in Fig. 2. Both the CPP and the WPP modes have their fields mainly concentrated at the apex of the V-groove on the interior and exterior walls respectively [Fig. 2(a) and 2(b)]. However, a local field maximum is also found on the opposite side of the walls for both modes. Hence, charge accumulation occurs at both metal-core and metal-cladding interfaces, giving evidence of the coupling between the inner and outer interfaces. As usual for plasmonic waves, the field amplitudes decay exponentially away from the interfaces. Judging from the field amplitude maxima at the core and cladding interfaces [Fig. 2(c) and 2(d)], it can be seen that the coupling across the film is much stronger for the CPP mode than for the WPP mode. This difference is a direct consequence of the so-called lightning rod effect (i.e charge accumulation) which only occurs at concave corners (wedge) but not at convex corners (groove) [24]. The two modes are characterized by orthogonal polarizations, the CPP being essentially transverse electric (with respect to the symmetry axis of the structure) and the WPP transverse magnetic. Their different field components exhibit opposite symmetries with respect to the symmetry axis, as could be expected from the charge distribution depicted in Fig. 1(b). Furthermore, it can be seen in Fig. 2(a) and 2(b) that for both modes, the longitudinal electric field E_z is symmetric across the metallic film while the transverse fields, E_x and E_y, change sign across the film as can be expected for symmetric charge distribution across the metal film.

#105456 - $15.00 USD Received 17 Dec 2008; revised 30 Jan 2009; accepted 30 Jan 2009; published 5 Feb 2009

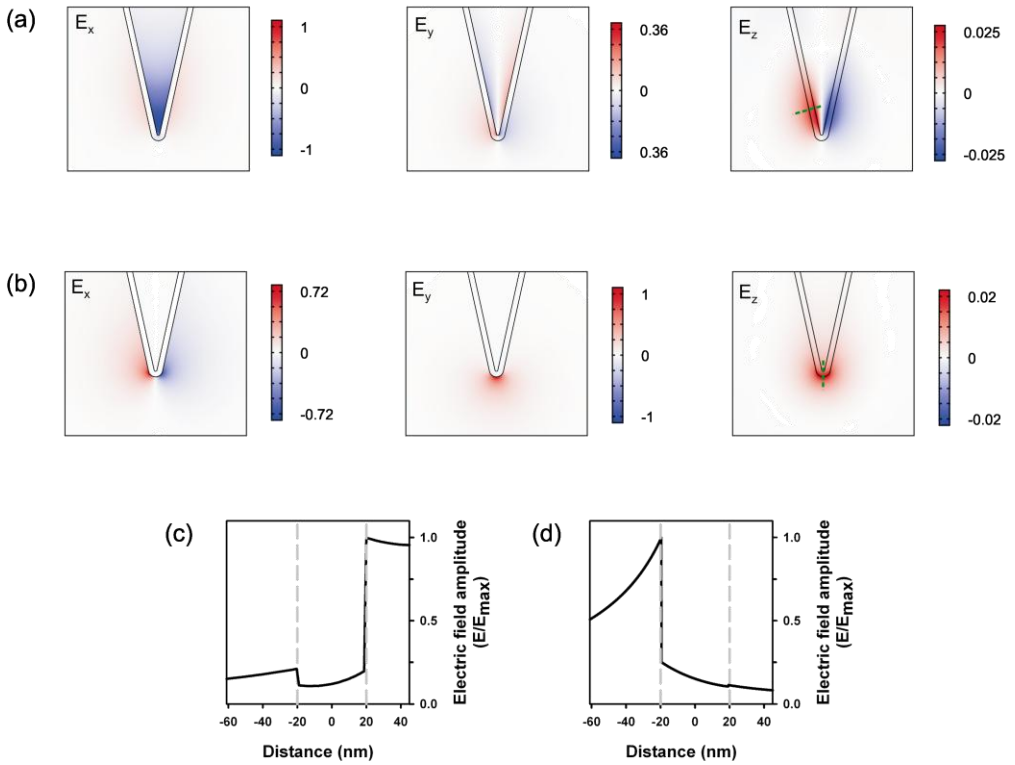

Fig. 2. (a) Distribution of the different components of the electric field near the tip for the CPP mode and (b) for the WPP mode of a 40nm-thick gold film. The magnitudes are normalized to the maximum of the dominant field component. (c) Cross-section of the electric field amplitude (normalized to the field maximum) measured perpendicularly to the metal film at the location of the field maxima (as shown by the green dashed line in (a) and (b)) for the CPP mode and (d) for the WPP mode.

In the following, we investigate how the CPP and WPP modes depend on the metal thickness and on their dielectric environment.

3. Symmetric environment

We first consider the behavior of the fundamental CPP mode when the gold thickness t is varied. The dispersion relations, modal areas A and propagation lengths are shown in Fig. 3(a) for different thicknesses. L_p is defined as the distance (along z) required for the intensity of the mode to decay by a factor e and we calculated A by evaluating the surface encompassed by the transverse positions for which the field amplitude has decayed by the same factor (see electric field isoline in green in the movies). A first remark is that the CPP mode remains confined for the whole set of parameters considered. The modal index of the CPP mode, n_{eff}, always exceeds the value of the refractive index of the cladding (i.e. air) and therefore the mode remains bound whatever the considered thickness. Furthermore, for any thickness t, n_{eff} is always greater than the effective index n_{SRP} of a SRP propagating on a gold film of similar thickness (not shown). Hence, the CPP mode stays confined in the groove and does not evolve into a SRP mode extending over the entire film, as can be the case for bulk metal when the wavelength becomes large compared to the groove depth or angle [13].

#105456 - $15.00 USD Received 17 Dec 2008; revised 30 Jan 2009; accepted 30 Jan 2009; published 5 Feb 2009

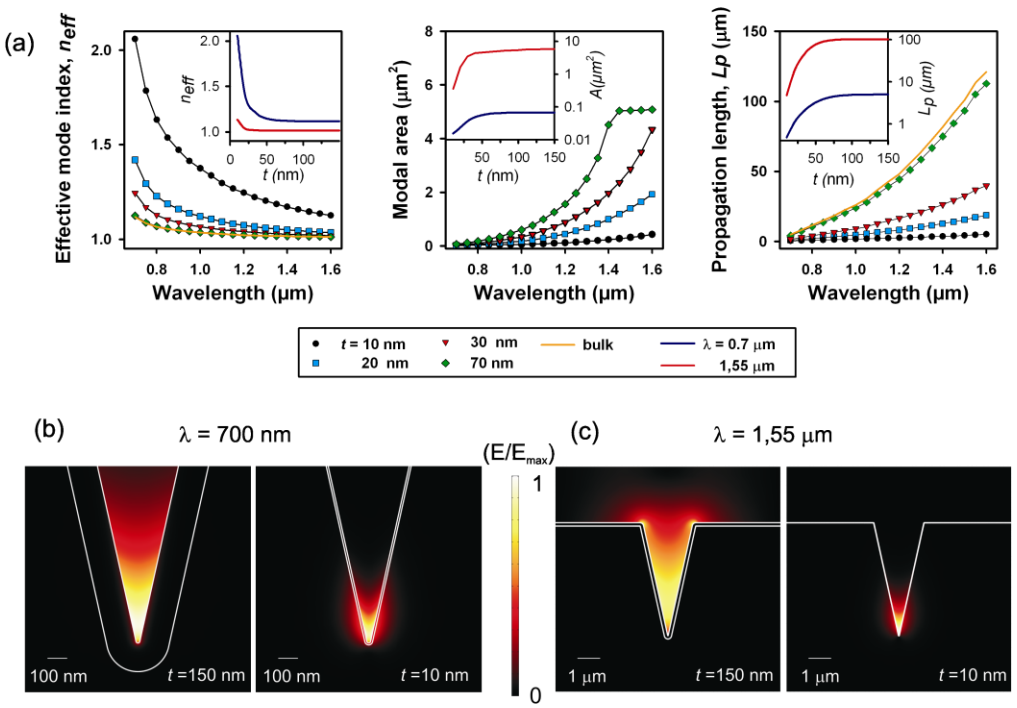

Fig. 3. (a) Modal properties of the CPP mode for different gold thicknesses: effective index n_{eff} (right), modal area A (center) and propagation length L_p (right). Insets show the evolution of these parameters as a function of t for two fixed wavelengths: 700 nm (blue) and 1,55 μm (red). (b) Evolution of the electric field distribution of the CPP with t at λ=700nm (close to tip) (Media 1). (c) Idem at λ =1,55 μm (Media 2).

For a given wavelength, we observe that n_{eff} increases considerably as the thickness decreases [inset Fig.3(a)], indicating that the fields are penetrating deeper into the metallic region similarly to what happens for symmetric SRP modes of thin films. For instance, at λ=700 nm (1.55μm), the fraction of energy located in the metal (computed using the Poynting theorem for dispersive media [25]) increases dramatically when t decreases, from 9% (2%) for the thicker film up to more than 30 % (25%) for the thinnest film. As a consequence, ohmic losses in the metal, which represent the dominant loss mechanism for the system considered in this paper, increase as t goes down. The propagation lengths L_p are seen to decrease accordingly with t in Fig. 3(a), from several wavelengths to roughly one wavelength in the visible and from several tens of wavelengths to only a few wavelengths in the infrared. In the opposite limit, when the thickness increases, the effective index and propagation lengths asymptotically approach the characteristic values of the CPP mode of a bulk V-groove (see insert of Fig. 3). This limit is reached more rapidly at longer wavelengths owing to the more efficient shielding of metals in the infrared.

The evolution of the modal area [Fig. 3(a)] and mode profile [Fig. 3(b) and 3(c)] clearly indicates that the increase in neff is associated with an improvement of the mode confinement in the vertical direction, the field being gradually squeezed towards the tip of the metallic groove. This is observed at all wavelengths, but could be particularly valuable for longer wavelengths. Indeed, when the wavelength increases the field expands considerably towards the entrance of the V-groove, giving rise to complex modal shapes caused by the hybridization of the CPP mode with corner modes [13]. When this occurs, the modal area A is seen to saturate [see the curve for t = 70 nm in Fig. 3(a)] as the field concentrates locally at the top corners. In such conditions, crosstalk between parallel waveguides can hardly be avoided in densely packed configurations. Decreasing the V-groove metal thickness could limit these

#105456 - $15.00 USD Received 17 Dec 2008; revised 30 Jan 2009; accepted 30 Jan 2009; published 5 Feb 2009

problems as can be seen in Fig. 3(c): as the field is pushed downwards, the hybridization with the corner modes becomes weaker and the CPP mode eventually returns to its original (non-hybridized) shape for the smallest thicknesses. It should however be noted that even though the mode remains mainly located in the gap region, it tends to lose its lateral confinement at the bottom of the groove as the coupling between core and cladding interfaces increases. Cross-sections in the field distribution (not shown) indicate that the skin depths in the dielectric core and cladding tend to decrease, confirming that the fields become more tightly bound to the metallic interfaces. In other words, the coupling through the metallic walls is favored at the expense of the coupling in the gap. As a result, the modal field is more equally distributed across the gold film and a non-negligible fraction of the modal power is carried by the cladding interface (around 20-30 % for the 10 nm film, depending on the wavelength).

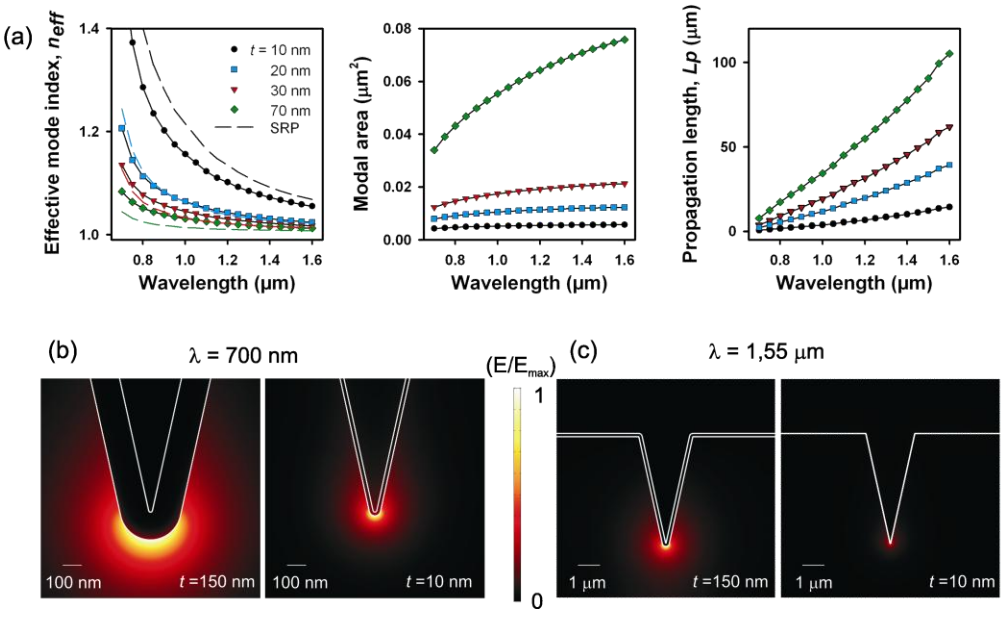

Fig. 4. (a) Modal properties of the WPP mode for different gold thicknesses: effective index n_{eff} (right), modal area A (center) and propagation length L_p (right). The dashed curves correspond to the short range surface plasmon mode (SRP) of an infinite thin gold film of the corresponding thickness. (b) Evolution of the electric field distribution of the WPP with t at λ=700nm, close to tip, (Media 3). (c) Idem at λ =1,55 μm (Media 4).

The behavior of the WPP mode, located at the opposite interface, follows the same trend as the CPP mode when the metal thickness decreases, as can be seen in Fig. 4. When t decreases, the modal field becomes more concentrated at the apex of the metallic tip [Fig. 4(b) and 4(c)], resulting in an increasing effective index n_{eff}, a decreasing propagation length L_p and a smaller modal area A [Fig. 4(a)]. We must however underline that both the thickness t and the radius of curvature r of the metal wall supporting the WPP mode are decreased in the simulation (see Fig. 1). Since the decrease of r is known to affect the modal properties of the WPP mode [14, 20], we performed a further set of simulations (not shown here) where r was kept fixed. The same trend was observed, thereby confirming the role of the metal thickness in this behavior. Despite the wider radius of curvature, we note that the WPP mode is more confined that the CPP mode especially at longer wavelengths where the WPP modal area is well below that of the CPP mode. This is also generally true for bulk structures.

On the other hand, the major difference regarding the thickness dependency is that the WPP mode maintains its modal shape much more efficiently as t decreases. Indeed, the WPP field remains mainly trapped at the core interface, with only a minor portion located at the

#105456 - $15.00 USD Received 17 Dec 2008; revised 30 Jan 2009; accepted 30 Jan 2009; published 5 Feb 2009

cladding interface. For instance, at λ = 700 nm and t = 20nm, only roughly 2.5% of the modal power is located in the cladding for the WPP mode compared to 20% for the CPP mode. This indicates a weaker coupling across the film for the WPP mode, as previously mentioned. In contrast to the CPP mode, we also note that for the smallest thicknesses considered (10 and 20 nm), the dispersion curve of the WPP mode goes below that of the SRP mode of an infinite gold film with similar thickness for specific wavelengths [see Fig 4(a)]. In this case, the WPP mode cannot be described anymore as a pure guided mode due to its leakage into the extended SRP mode. However, the mode profiles, shown in Fig 4(b) and 4(c) indicate that the modal field remains essentially confined at the tip apex. The coupling of the wedge mode with the extended SRP is indeed very weak, given that their main field component are quasi orthogonal (a situation that will obviously change if the groove angle is increased). It can only be detected in the weakest part of the mode profile (for which the electric field amplitude has decayed below one tenth of its maximum value, E<Emax/10). As the dispersion curve of the WPP mode goes below that of the SRP mode, oscillations of the field intensity are observed along the side walls, indicating reflections from the top corners. In other words, the WPP mode hybridizes with high-order modes of the strip-like SRP modes supported by the groove walls [hence its dispersion curve crosses the dispersion curve of these high-order modes which lies below that of the *slab* SRP [26], shown in Fig.4(a)]. This coupling is, however, very weak given the field symmetry mismatch and the overall effect of the decreasing thickness is dominated by the compression of the mode fields at the wedge apex and the consequent increase of losses.

Altogether, our simulations clearly show that the use of a finite metal thickness reduces both the CPP and WPP modal volume by increasing the field concentration at the metallic interfaces. However, this improvement of the confinement is obtained at the expense of higher losses in the metal.

3. Asymmetric environment

In this section, we study the influence of the dielectric contrast between the core and the cladding media on the propagation characteristics and existence conditions of the CPP and WPP modes.

Let us first focus on the CPP mode and gradually increase the dielectric permittivity of the lower dielectric medium (cladding) ε_2 while the dielectric permittivity ε_1 of the upper medium (core) is kept constant. The free space wavelength is set to 700 nm or 1,55 μm and the numerical simulations are again performed for various thicknesses. The dispersion curves (n_{eff} vs ε_2), modal area and propagation lengths of the CPP mode are presented in Fig. 5, together with the curves corresponding to the bound SRP of a metallic slab in a similar asymmetric environment. In Fig. 5(a) and 5(b), we can see that the dispersion curve of the CPP mode approaches that of the SRP as the dielectric contrast increases. For the smallest thickness (10nm), the CPP modal index remains above the SRP dispersion curve (at least for the range of dielectric contrast considered) and the mode remains well confined at the groove apex. On the other hand, for slightly thicker films (t>10nm), the CPP dispersion curve is seen to merge with the SRP curve as ε_2 reaches a critical value (depending both on the considered wavelength and thickness). This indicates that the CPP mode leaks into a strip-like SRP mode delocalized on the side walls.

#105456 - $15.00 USD Received 17 Dec 2008; revised 30 Jan 2009; accepted 30 Jan 2009; published 5 Feb 2009

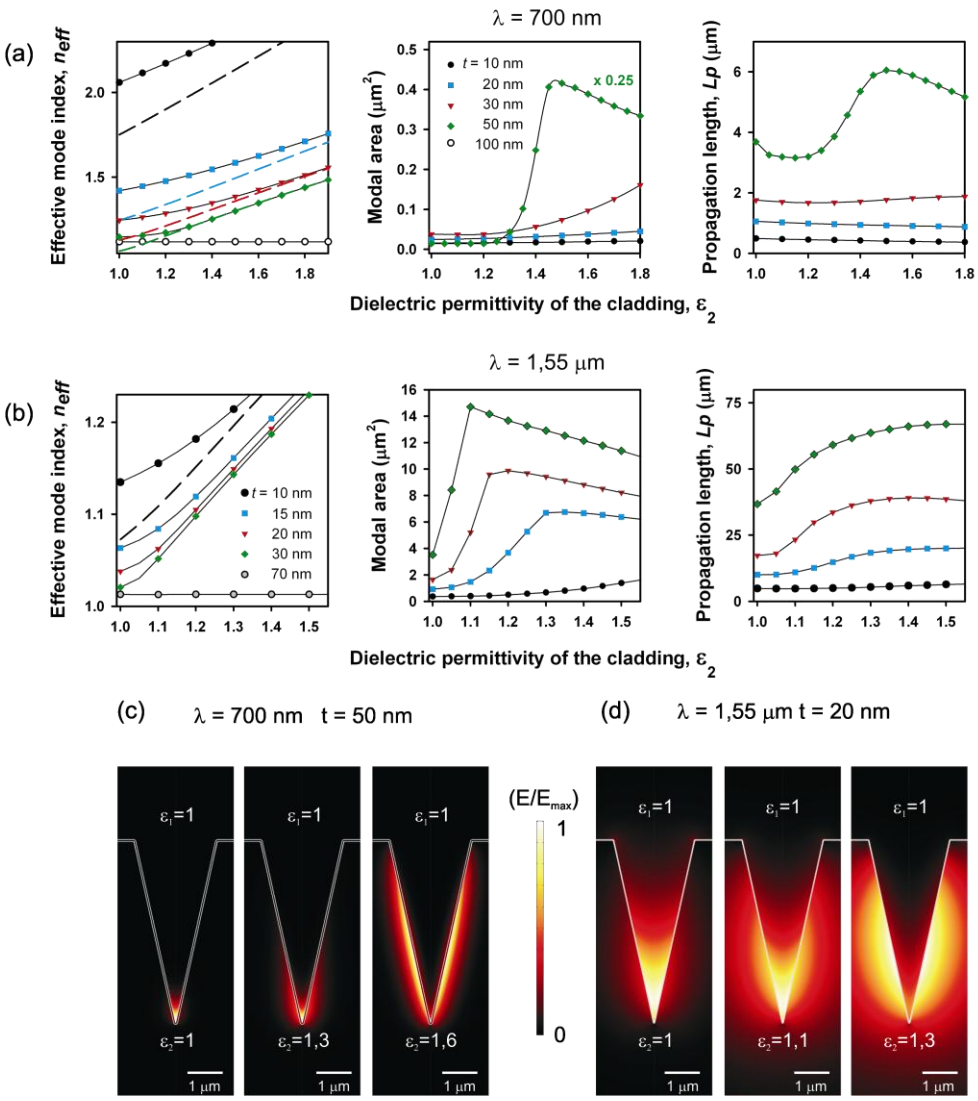

Fig. 5. Modal properties of the CPP mode as a function of the dielectric constant of the substrate ε_2 at λ = 700 nm (a) and λ = 1,55 μm (b): effective index n_{eff} (right), modal area A (center) and propagation length L_p (right). The dashed curves correspond to the short range surface plasmon mode (SRP) of an infinite thin gold film of the corresponding thickness. (c) Evolution of the mode profile with ε_2 at λ = 700 nm for t=50 nm (Media 5). (d) Idem at λ = 1,55 μm for t= 20 nm (Media 6).

The evolution of the mode profile with ε_2 (for a given thickness), as shown in Fig. 5(c) and (d) for t = 50 nm (λ=700nm) and 20 nm (λ=1.55 μm), provides a better understanding of the modal behavior as the transition between CPP and delocalized SRP occurs. As ε_2 increases, the field is gradually expelled from the core, starting at the bottom of the groove and stretching progressively along the outside walls, taking the form of two uncoupled SRP modes bound by the top and bottom corners. This change in character of the mode is associated with a complex redistribution of the modal energy which is clearly visible in the modal area and propagation plots [Fig. 5(a) and 5(b)]. For small dielectric contrasts, the fields essentially expand laterally through the metallic film (as evidenced by the rise of A) and the

#105456 - $15.00 USD Received 17 Dec 2008; revised 30 Jan 2009; accepted 30 Jan 2009; published 5 Feb 2009

fraction of energy located in the metal grows (leading to a decrease of L_p) until the modal energy in the core and cladding become equal. As the field continues to escape from the gap and expand along the cladding interface, the modal energy keeps on growing in the cladding while it decreases in both the core and the metal, resulting in a small increase of the propagation length. Finally, as ε_2 is further increased, the mode completely loses its localized character and turns into two decoupled SRP modes as the field concentration at the bottom of the groove disappears. The modal area then decreases and the losses grow again with ε_2 as expected for the bound SRP mode of a slab in such an asymmetric environment [23].

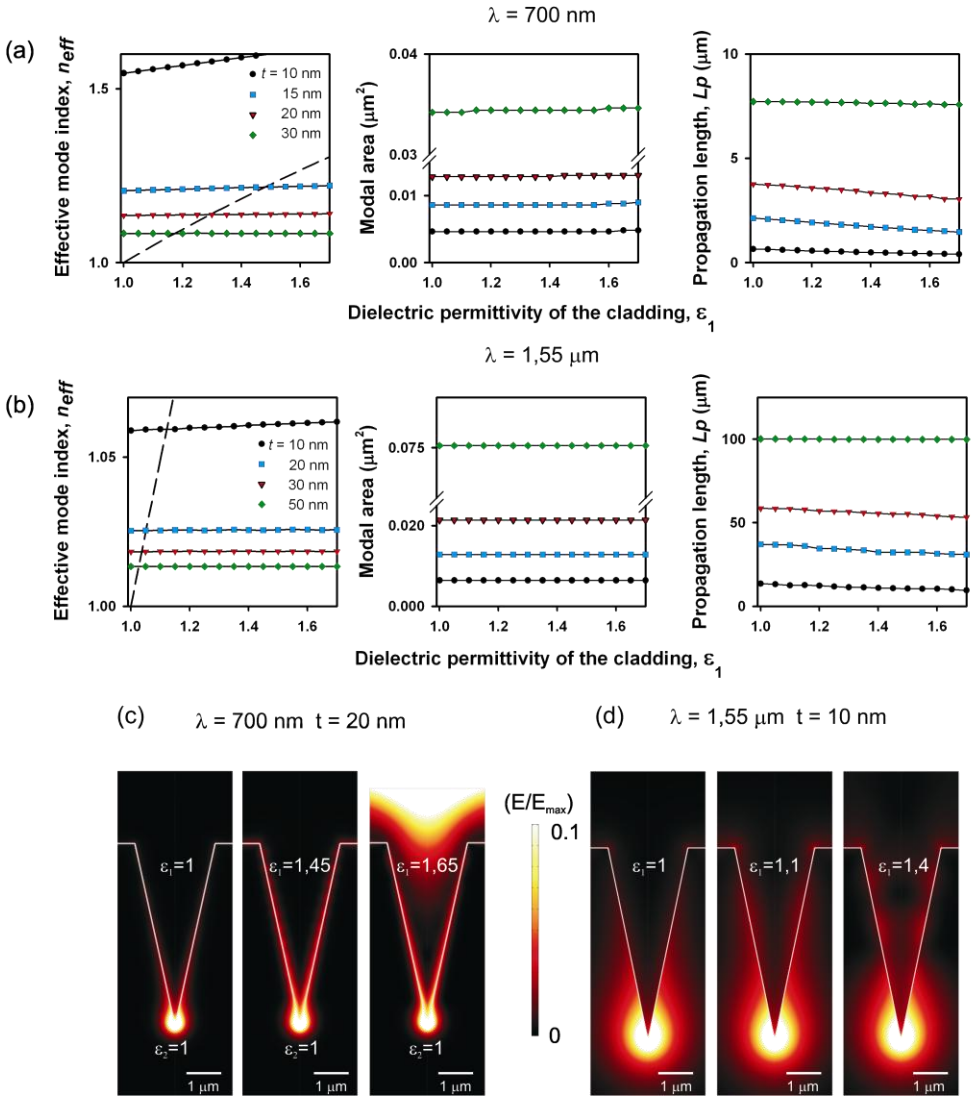

Fig. 6. Modal properties of the WPP mode as a function of the dielectric constant of the substrate ε_2 at λ = 700 nm (a) and λ = 1,55 μm (b): effective index n_{eff} (right), modal area A (center) and propagation length L_p (right). The dashed curves correspond to the light line in the cladding. (c) Evolution of the mode profile with ε_2 at λ = 700 nm for t=20 nm (Media 7). (d) Idem at λ = 1,55 μm for t= 10 nm (Media 8).Note that the color scale is saturated at $E_{max}/10$.

#105456 - $15.00 USD Received 17 Dec 2008; revised 30 Jan 2009; accepted 30 Jan 2009; published 5 Feb 2009

The dispersion curves in Fig. 5 also show that the degree of asymmetry allowing the existence of pure CPP modes increases with decreasing metal thickness, since the CPP and SRP dispersion curves meet at higher values of ε_2. Although the fields are more spread out between the core and cladding for the thin films, they are also more tightly bound to the groove apex and therefore less likely to delocalize along the groove walls when the asymmetry increases. In the opposite limit, i.e. when the gold thickness gets larger than the mode penetration depth in the metal, the mode becomes insensitive to the cladding index and n_{eff} remains constant [see t = 100 nm at λ = 700 nm or t = 70 nm at λ = 1.55 μm in Fig. 5(a)]. Finally, we can see that the CPP mode leaks more rapidly into SRP modes at higher wavelengths as the fields tend to be more delocalized and the difference between n_{eff} and n_{SRP} becomes smaller.

The behavior of the WPP with respect to its dielectric environment is quite different from that of the CPP mode as can be seen in Fig. 6. Indeed, no cut-off is found in this case when the dielectric permittivity of the cladding ε_1 is varied. Although we can observe a weak leakage of the CPP mode along the side walls due to its coupling with the SRP modes located at the metal-cladding interface, most of the field remains confined at the groove tip. As a consequence, the properties of the CPP mode are fairly insensitive to the dielectric asymmetry. The effective index and modal area only grows moderately with ε_1 due to the small leakage and the losses in the metal slightly increase [Fig. 6(a) and 6(b)].The main change observed in the mode profile when n_{eff} grows is the increasing number of oscillations in the small field amplitude measured along the side walls, indicating that the WPP mode hybridizes (weakly) with strip-like SRP modes of increasing order. Once again, this hybridization is very weak and the lack of efficient coupling between the WPP mode and the SRP mode can be explained by the asymmetry of their respective modal field (the electric field of the WPP mode being mainly *y*-polarized while that of the SRP mode is mainly *x*-polarized as a consequence of the sharp groove angle). We note that this situation will change if the groove angle becomes wider since the *x*-component of the SRP mode electrical field would grow at the expense of its *y*-component). For thicknesses t above 10 nm, we observe that the WPP dispersion curves cross the light line and therefore start to leak radiatively in the substrate. This is indeed confirmed by the mode profiles [Fig.6(c) and 6(d)] which show some fraction of the electric field radiating away from the groove as the light line is crossed.

4. Conclusion

The channel and wedge plasmon polariton modes guided by a V-groove structure of finite metal thickness have been characterized and their behavior with respect to the metal thickness and dielectric environment has been investigated. The results indicate that a reduction of the metal thickness induces a considerable diminution of the modal volume for both the CPP and WPP modes, as well as an increase of their propagation losses. This behavior stems from their characteristic charge distributions which are found to be symmetric across the metal film in both cases. The effect of a dielectric contrast between the media supporting the V-groove is found to affect the two modes in different ways. As the asymmetry increases, the CPP mode evolves into two decoupled SRP modes delocalized along the groove walls with their field mainly located at the cladding interface. On the other hand, the WPP mode is relatively insensitive to the dielectric asymmetry, maintaining its modal shape before leaking into the cladding medium as the dielectric contrast reaches a critical value which depends on the metal thickness and wavelength. These results allow for the optimal design and fabrication of CPP and WPP waveguides using a variety of thin film nanotechnologies.

Acknowledgments

Funding from the Swiss National Competence Center in Research “Nanoscale Science” is gratefully acknowledged.

#105456 - $15.00 USD Received 17 Dec 2008; revised 30 Jan 2009; accepted 30 Jan 2009; published 5 Feb 2009